Received: 12 January 2023 | Revised: 15 April 2024 | Accepted: 15 April 2024

DOI: 10.1111/joa.14053

Journal of Anatomy ANATOMICAL SOCIETY WILEY

ORIGINAL ARTICLE

Histological analysis and etiology of a pathological iguanodontian femur from England

Filippo Bertozzo[1,2] | Koen Stein[3] | Elena Varotto[4,5] | Francesco M. Galassi[6] | Alastair Ruffell[7] | Eileen Murphy[7]

[1]Operational Directorate Earth and History of Life, Royal Belgian Institute of Natural Sciences, Brussels, Belgium

[2]Sociedade de Historia Natural, Torres Vedras, Portugal

[3]Vrije Universiteit Brussel, Brussels, Belgium

[4]Archaeology, College of Humanities, Arts and Social Sciences, Flinders University, Adelaide, South Australia, Australia

[5]FAPAB Research Center, Avola (SR), Sicily, Italy

[6]Department of Anthropology, Faculty of Biology and Environmental Protection, University of Lodz, Lodz, Poland

[7]School of Natural and Built Environment, Queen's University Belfast, Belfast, Northern Ireland, UK

Correspondence
Filippo Bertozzo, Operational Directorate Earth and History of Life, Royal Belgian Institute of Natural Sciences, Brussels, Belgium.
Email: filippo.bertozzo@gmail.com

Funding information
Horizon 2020 research and innovation programme under the MSCA grant agreement, Grant/Award Number: 754507

Abstract

Derived ornithopods, such as hadrosaurids, show a high occurrence of fossilized lesions and diseases. However, paleopathologies in iguanodontians seem to be less common, considering the rich fossil record of these taxa in Europe, in particular in Belgium, Britain and Spain. Here, we describe an iguanodontian femur discovered in England that exhibits a large overgrowth of its lateral aspect, not previously recognized in any other similar remains. The specimen was scanned with micro-computed tomography (microCT) and later sectioned in three sites of the overgrowth for histological analysis. The femur belongs to an early adult Iguanodontia indet., based on the presence of a woven parallel fibered complex in the outer cortex and three to four lines of arrested growth. Internal analysis of the dome-like overgrowth suggests it can be diagnosed as a fracture callus. The injury might have negatively impacted upon the animal's locomotion as the trauma had occurred in the region above the knee, a crucial spot for hindlimb musculature. Finally, a cancellous medullary bone-like tissue was recognized in the medullary cavity next to the pathological overgrowth. An attempt was made to determine the precise nature of this tissue, as medullary bone is linked with the ovulation period in (avian) dinosaurs, whereas other types of endosteal, medullary bone-like tissue have previously been recognized in pathological bones.

KEYWORDS
Dinosauria, locomotion, medullary bone, Ornithopoda, paleopathology

1 | INTRODUCTION

Paleopathology, or the study of fossilized lesions and diseases, and the associated implications for the biology and lifestyles of dinosaurs have gained increased momentum over the past 50 years (e.g. Bertozzo et al., 2021; Hanna, 2002; Tanke & Rothschild, 2014; Tschopp et al., 2014). Analysis of an increasingly growing database of pathological specimens from across the entire clade of Dinosauria has enabled new knowledge to be gained about their healing processes (e.g. Bertozzo et al., 2021; Hunt et al., 2019), locomotion (e.g. Cruzado-Caballero et al., 2020), lifestyle (e.g. Foth et al., 2015; Hamm et al., 2020; Hanna, 2002; Senter & Juengst, 2016; Słowiak et al., 2021) and even behavior related to pathological trends (e.g. Bertozzo, Dal Sasso, et al., 2017; Brown et al., 2021; Farke et al., 2009; Gutherz et al., 2020; Peterson et al., 2013). The development of new analytical techniques, together with the assistance of novel medical devices, is also contributing to the establishment of a more precise and refined diagnosis in vertebrate paleontology (e.g. Anné et al., 2016; Bertozzo et al., 2022; Hedrick et al., 2016; Peterson et al., 2013). During the early stages of vertebrate paleopathology, fossilized injuries and abnormal conditions were solely described morphologically (e.g. Moodie, 1923), often resulting in an

inaccurate identification (see Rothschild & Berman, 1991). However, over the past 30 years, the advent of tomographic pictures via CT scan, microCT scan and synchrotron have offered a unique opportunity to compare the gross external morphology of lesions to their inner characteristics. Several authors have highlighted the importance of these analyses for paleopathological studies of dinosaur remains, including diagnoses of traumatic fractures (Butler et al., 2013; Farke & O'Connor, 2007; Foth et al., 2015; Hedrick et al., 2016; Hunt et al., 2019; Peterson & Vittore, 2012; Siviero et al., 2020; Straight et al., 2009), stress bioproducts (Gonzalez et al., 2017; Tschopp et al., 2014), Schmorl's nodes (Witzmann et al., 2016), the sequelae of infection (García et al., 2017; Hamm et al., 2020; Hunt et al., 2019), septic arthritis (Anné et al., 2016), spondyloarthropathy (Martinelli et al., 2015), a range of neoplasms including, ameloblastoma (Dumbravă et al., 2016), Langerhans cell histiocytosis (Rothschild et al., 2020), osteosarcoma (Ekhtiari et al., 2020), osteoma and hemangioma (de Souza Barbosa et al., 2016). In some instances, it is possible to gain additional data through paleohistology, a more intrusive, yet crucial, type of analysis for facilitating reliable diagnoses of trauma, infection and tumors (e.g. Griffin, 2018; Hamm et al., 2020; Hedrick et al., 2016; Jentgen-Ceschino et al., 2020; Redelstorff et al., 2014). Histological analyses not only provide information about externally visible anomalies but also detect lesions within bones with an apparently healthy external appearance, as recently reported by Jentgen-Ceschino et al. (2020). Histological sections allow researchers to analyze bones at a microstructure level at a definition not yet reached through analysis of CT scans.

In this research, the bone tissue evident in a dome-like overgrowth on the lateral side of the Iguanodontia indet. femur NHMUK PV R6609 is described at macroscopic (gross morphology) and microscopic (CT scan and histology) levels. The specimen is a stout, columnar bone that suffered a significant antemortem trauma on the lower part of the hindlimb. The aims of the study are to: (i) assign the specimen to a proper taxon; (ii) determine whether the animal was subadult or a full adult when the trauma occurred; (iii) investigate how the bone reacted to the injury and if it was still healing at the time of death and (iv) identify the possible presence of secondary infection.

Institutional abbreviations: NHMUK, Natural History Museum of London, England, UK and QUB, Queen's University Belfast, Northern Ireland, UK.

2 | MATERIALS AND METHODS

NHMUK PV R6609 is a femur of an Iguanodontia indet. (Dinosauria, Ornithischia) from the Weald Clay Formation of Smokejacks Quarry (Barremian: Ockley, Surrey, England), acquired in January 1951 by the Natural History Museum of London as part of the W.H.E. Rivett Collection. The pathological nature of the overgrowth, located on the distal craniolateral surface of the distal end of the shaft, was recognized during a paleopathological survey undertaken at the NHMUK as part of a doctoral research project (FB). The bone was photographed using a Sony Mirrorless a5100 (exposure time 1/60 s, ISO 1000, focal length 16 mm, maximum aperture of 3.617), with a scale bar of 10 cm, virtually obtained using the free software ImageJ®. The pathological area displayed a swollen dome-like structure, an anomalous feature compared to other iguanodontian femora from England (Filippo Bertozzo, personal observation) and Belgium (Norman, 1980, 1986). To confirm the pathological nature of the structure, three histological transverse sections were taken: (1) on the unaffected part of the diaphysis (the area between the fourth trochanter and the beginning of the overgrowth); (2) at the start of the overgrowth, where the bone surface started to rise and (3) at the apex of the overgrowth, placed at its midpoint (Figure 1). Since the technique is destructive, a 3D-model of the bone was initially created via surface scanning using a Faro ScanArm LLP (Laser Line Probe). The data was captured using Geomagic Wrap software and processed with the same software. The capture setting was used by default to a resolution of 0.01 in (space between captured points) and the final model file has been decimated by 20% to simplify the mesh structure and make the file usable. The specimen was also scanned using a Nikon HMX 225 ST at the Imaging and Analysis Centre of the NHMUK. The CT data was processed using Avizo 3D 2021.1.

The histological samples were prepared at NHMUK. During initial sectioning, the femur fractured into several pieces and was

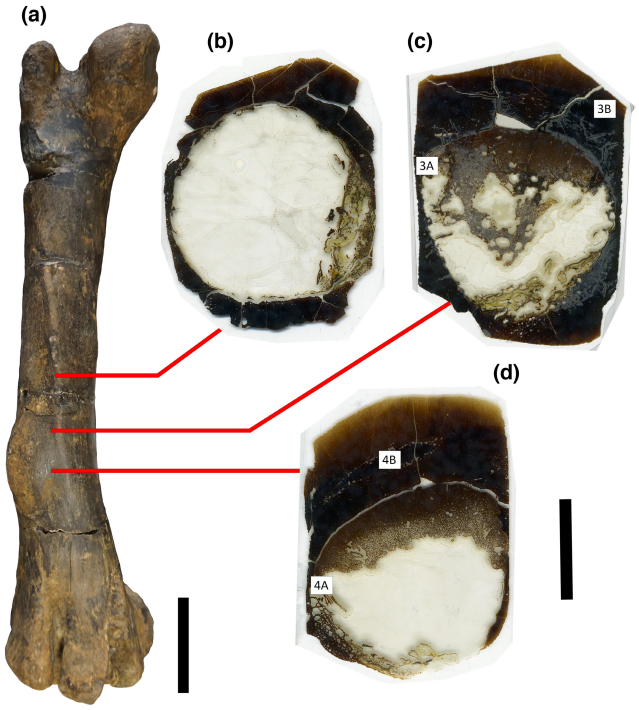

FIGURE 1 (a) Cranial view of the pathological femur NHMUK PV R6609. The three lines correspond to the three cuts and histological sections. (b) Section "A" taken in the apparently "healthy" portion of the shaft. (c) Section "B" at the proximal region of the dome-like overgrowth. (d) Section "C" in the middle of the dome-like overgrowth. The white squares correspond to histological sections in Figures 3 and 4. Scale bars = 10 cm (a) and 2 cm (b–d).

subsequently reconstructed using KEP epoxy resin, prior to embedding it in the same resin to prevent further damage. The different components of the femur were embedded by standing them upright in a plastic container which was then filled with resin. The resin was left to harden for 2 days, after which it was mounted and cut in three different transverse levels (Figure 1). The surface of each section was polished by grinding using a 120 μm grade disk, followed by lapping the surface using 800 grade fixed abrasive paper. Once the surface had been prepared, the samples were mounted on glass slides using KEP epoxy resin and kept under pressure using a jig while the resin set. The sections were left overnight to allow the resin to rest and fix. The excess material was cut away and the sections were ground to 200 μm above their final thickness using Geoform, a machine with both a saw and grinding wheel built into either side of it. The sections were then lapped with 600 grade carborundum using a Logitech LP50 down to 60 μm thickness. Each section was checked to ensure it was the correct thickness under a petrographic microscope before the cover slip was applied using Loctite AA358 UV resin, and further checked for air bubbles under a petrographic microscope. Following this, the sections were put under a UV lamp for 3 s to partially cure the resin. Any excess resin around the edges of the cover slips was removed using a scalpel. The sections were then put under the UV lamp again for 1 min to fully set the resin. The final slides were analyzed with a Zeiss Axioscope polarized light microscope using Zeiss ZEN imaging software at Vrije Universiteit Brussel. The specimen, CT scans, and thin sections of the femur NHMUK PV R6609 are all curated in the collections of the Natural History Museum, London. Osteohistological terminology was based on de Buffrénil and Quilhac (2021).

3 | RESULTS

3.1 | Osteological description

NHMUK PV R6609 is a right femur from a mid-sized ornithopod, referred to Iguanodontia indet. The bone is 72 cm long, measured from the most proximal aspect of the femoral head to the most distal margin of the condyles. The shaft width of the femur remains constant along the length of the specimen. The proximal portion of the shaft is straight, but below the fourth trochanter it is curved caudally. In caudal view, the femur is also slightly bowed (Figure 2). Prominent curvature of the femur is a characteristic identified in dryosaurids, *Camptosaurus dispar*, *Draconyx loureiroi*, *Barilium dawsoni*, *Altirhinus kurzanovi*, *Probactrosaurus gobiensis* (McDonald, 2012), and *Mantellisaurus atherfieldensis* (McDonald, 2012; Norman, 1986) and observed to be variably present (together with the straight morphology) in *Iguanodon bernissartensis* (Verdú et al., 2017). The head of the femur is prominent, wide and ball-shaped, set at 146° to the shaft, and supported by a thick and strong neck. A wide and deep groove separates the head of the femur from the greater trochanter, similar to the morphology in *Ouranosaurus nigeriensis* (Bertozzo, Dalla Vecchia, et al., 2017). The greater trochanter is wider than the femoral head, and the lateral surface is grooved by longitudinal striations for the insertion of *M. ischiotrocantericus* (Maidment & Barrett, 2012), the complex of *M. ischiotrocantericus* and *M. iliofemoralis* (Dilkes, 2000), or *M. iliotrochantericus* (Norman, 1986). A faint bulge arises from the caudolateral surface of the greater trochanter. The lesser trochanter is not preserved and was detached from the femur, possibly during fossilization. The original shape can be reconstructed from the broken portion of the prominent ridge that runs downwards and diagonally towards the distomedial side of the femur, above the medial condyle. It is well-developed, hence differing from the femora of *I. bernissartensis* (Norman, 1980), *M. atherfieldensis* (Norman, 1986), *Eolambia caroljonesa* (McDonald et al., 2012) and *O. nigeriensis* (Bertozzo, Dalla Vecchia, et al., 2017). Based on the curvature of the ridge, the lesser trochanter would have been prominent, as evident in *M. atherfieldensis*. The fourth trochanter is missing, potentially detached during fossilization, but it would have been quite thick (e.g. Norman, 1980, 1986). It is located slightly below the mid-section of the femur, more similar to that of *I. bernissartensis* (Norman, 1980), *M. atherfieldensis* (Norman, 1986), *Eolambia caroljonesa* (McDonald et al., 2012) and *O. nigeriensis* (Bertozzo, Dalla Vecchia, et al., 2017) than in *Probactrosaurus gobiensis* (Norman, 2002), *Tethyshadros insularis* (Dalla Vecchia, 2009) and *Bactrosaurus johnsoni* (Godefroit et al., 1998). The distal area of the femur is characterized by two prominent condyles. The medial one is the larger, and they are separated by a U-like cranial intercondylar groove, and a narrow caudal one, partially closed by a lateral projection of the medial condyle. In cranial view, the medial condyle is taphonomically displaced, forming a wide "scar" that shifted its lateral portion next to the lateral condyle. In medial view, the outline of the medial condyle resembles the wide and nearly horizontal one of *I. bernissartensis* more so than the strongly curved condyle of *M. atherfieldensis* (Norman, 1980, 1986). Finally, a well-formed dome-like overgrowth is evident on the lateral surface above the distal region, where the femur bends caudally.

3.2 | Paleopathological description

3.2.1 | Morphological analysis

The dome-like overgrowth is located on the distal craniolateral portion of the femur (Figures 1 and 2c,d). The margins are contiguous with the normal bone surface of the shaft. The surface of the dome is slightly irregular, but no draining sinuses are observed. The overgrowth is subcircular in lateral view, developing more proximodistally than cranio-caudally, and the lateral surface has a flattened appearance in medial view. Externally, the overgrowth does not show definitive signs of an infectious or neoplastic process.

3.2.2 | Histological analysis

At the histological level, the lesion is clearly recognizable through the three sections taken. Section "A" represents the apparently "healthy"

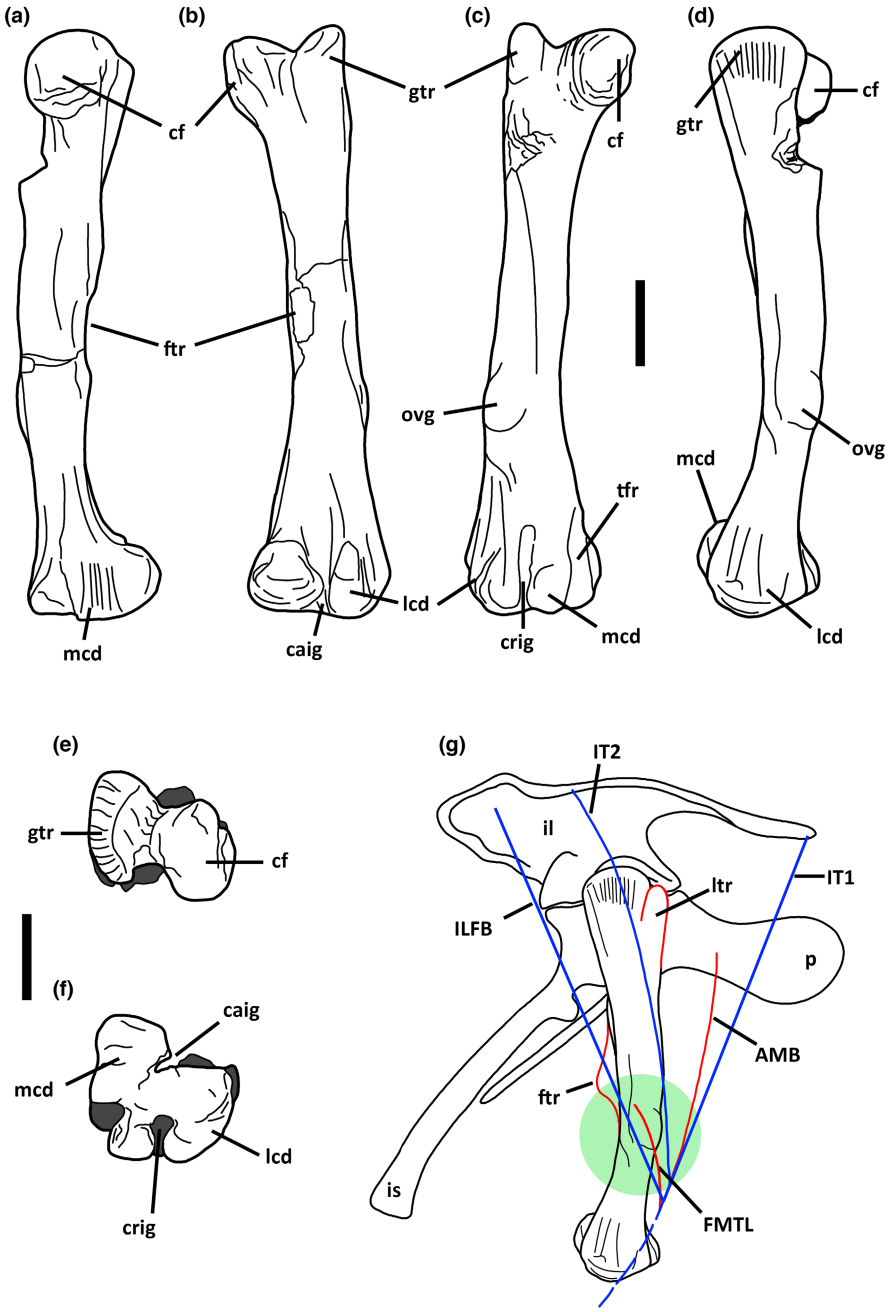

FIGURE 2 Drawing of the pathological femur NHMUK PV R6609 in medial (a), caudal (b), cranial (c), lateral (d), proximal (e) and distal (f) views. The pelvic and muscular reconstruction of *Mantellisaurus atherfieldensis* from Norman (1986) are used as a basis for reconstructing the articulation of NHMUK PV R6609 (g). The original fourth trochanter and the lesser trochanter are reconstructed based on *M. atherfieldensis* (Norman, 1986). The green circle corresponds to the pathological area. AMB, *M. ambiens*; caig, caudal intercondylar groove; cf, caput femoris (head of the femur); crig, cranial intercondylar groove; FMTL, *M. femorotibialis*; ftr, fourth trochanter; il, ilium; ILFB, *M. iliofibularis*; is, ischium; IT1, *M. iliotibialis 1*; IT2, *M. iliotibialis 2*; lcd, lateral condyle; ltr, little trochanter; mcd, medial condyle; ovg, overgrowth; p, pubis; tfr, taphonomical fracture. Scale bars = 10 cm.

unaffected part of the femur (Figure 1a). A large medullary cavity opens at the center, and the bone tissue is composed of two generations of secondary osteons (Mitchell et al., 2017) (Figure 3a).

The plexiform primary bone contains well-developed primary osteons. We did not observe any external fundamental system (EFS); however, the primary bone shows an overall maturity and numerous secondary osteons that decrease in number moving from the internal area to the surface. Section "B" corresponds to the proximal region of the dome-like overgrowth (Figure 1c). The medullary cavity contains an endosteal woven bone tissue (Figures 3a and 4a), characterized by a high density of irregularly shaped osteocyte lacunae, high vascularity and a cancellous structure. However, the general appearance of this tissue differs from the endosteal bone that surrounds the medullary cavity (Figure 4a). An inner circumferential

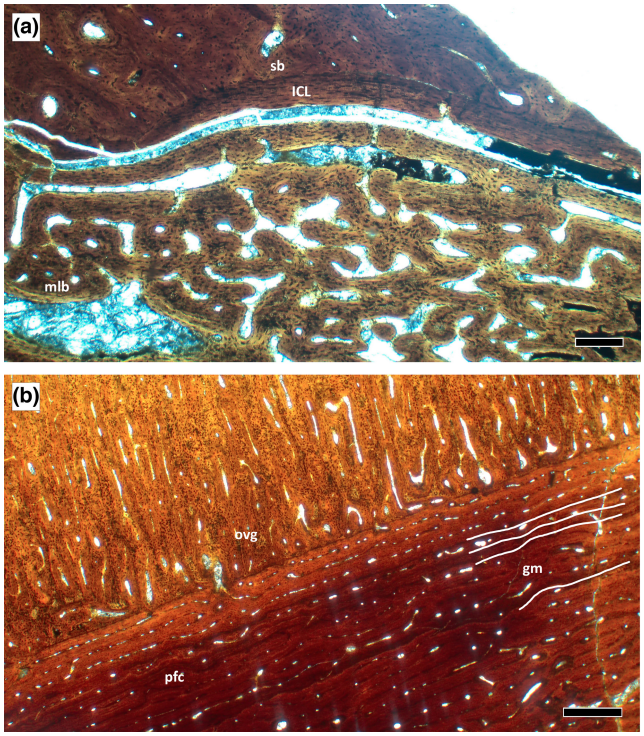

FIGURE 3 (a) The clear separation between the secondary bone of the inner cortex and the medullary bone-like tissue filling the medullary cavity. (b) Area of transition between the original cortex, formed by the parallel fibered complex with scattered secondary osteons, and the reactive woven bone of the periosteal overgrowth. gm, growth marks (marked as white lines in b); ICL, inner circumferential layer; mlb, medullary bone-like tissue; ovg, overgrowth; pfc, parallel fibered complex; sb, secondary bone. Scale bars = 500 μm.

layer (ICL) of lamellar bone (Figure 3a) separates this endosteal bone from the inner cortex along the entire margin of the section, as demonstrated by a disruption in the lacunocanalicular system. The outer cortex is composed of secondary bone, formed initially by tightly packed secondary osteons. Two generations of osteons are recognized. Following Mitchell et al. (2017), this conforms to a remodeling stage 3, however, considering the obvious pathological state of the specimen, identification of the remodeling stage may be affected by the lesion.

In the outermost region of the outer cortex, the osteons are more scattered within a laminar–plexiform primary bone, that shows clear woven parallel fibered complex features close to the external margin of the periosteum (Figure 3b). The periosteal reactive bone deposition is much more extensive and clearly visible in Section "C" (Figure 1d). This section is taken from the middle region of the dome-like overgrowth, and it overlaps the cortex (Figure 3b). The overgrowth is formed predominantly by primary osteons with few scattered secondary osteons located near the cortex (Figure 3b). Within one region of the superficial cortex, there is a 2.5 cm long focus of cortical bone that is disrupted and partially separated circumferentially from the surrounding adjacent cortex. This creates a discontinuous island of cortical bone entrapped within its surroundings (Figures 4b and 5), and likely occurred as a result of the trauma. This region consists of a lens-shaped area of parallel fibered bone (herein referred to as "lens"), located between the outer cortex and the periosteal overgrowth in Section B (Figures 4b and 5), and is also clearly visible in the CT scans (Figure 6a,b).

Along the margin of this "lens," areas of resorption cavities disrupt the contour of the structure. A total of three, perhaps four, growth lines (sensu Woodward et al., 2015; Wosik et al., 2020; Wosik & Evans, 2022) are recognized in thin section (Figure 3b) similar to what can be observed in hadrosaurids (Woodward et al., 2015), but a precise comparison and growth rate analysis is beyond the scope of the current study.

4 | DISCUSSION

4.1 | Species, differential diagnosis, and healing status

The size and morphology of the element and the histological analysis revealed that the iguanodontian femur likely belonged to an early adult (cf. Wosik et al., 2020; Wosik & Evans, 2022). The external morphology resembles that of *Mantellisaurus atherfieldensis* (Norman, 1986) in relation to the caudal curvature of the distal half and the prominent lesser trochanter (based on the curvature of its remaining basal portion). However, the shape of the medial condyle is more similar to that of *Iguanodon bernissartensis* (Norman, 1980), being mostly horizontal and not as strongly curved as in *M. atherfieldensis*. Overall, the femur seems to show an intermediate morphology between the two iguanodontian species but, because of its isolated nature, it is regarded as Iguanodontia indet.

The plexiform primary bone contains well-developed primary osteons. We did not observe any EFS, but the stage of remodeling and presence of numerous secondary osteons (that decrease in number moving from the internal area to the surface) suggests the individual was almost fully grown (cf. Woodward et al., 2015).

The pathological overgrowth is located on the distal craniolateral surface of the femur, precisely at the location where the distal half curves caudally (Figure 2c,d). Such raised dome-like structures can typically be caused by trauma, infection or tumors (Cruzado-Caballero et al., 2021).

Primary benign and malignant bone tumors that can cause expansile or disruptive growths in the long bones include osteoma, osteoid osteoma, osteoblastoma, osteochondroma, chondromyxoid fibroma, fibrous dysplasia, aneurysmal bone cyst, and osteosarcoma among others. These were considered as possible differential diagnoses for this lesion but, since none of these exhibited similar gross, CT or histological features, they were subsequently ruled out as a possible cause. One alternative interpretation is ossified hematoma, but it is a rare condition, associated with dystrophic mineralization of a hematoma (i.e. subdural hematoma in Mansour et al., 2023), showing different radiological and histological features, without creating abundant perpendicularly oriented reactive new woven bone tissue. The regular morphology of the dome-like

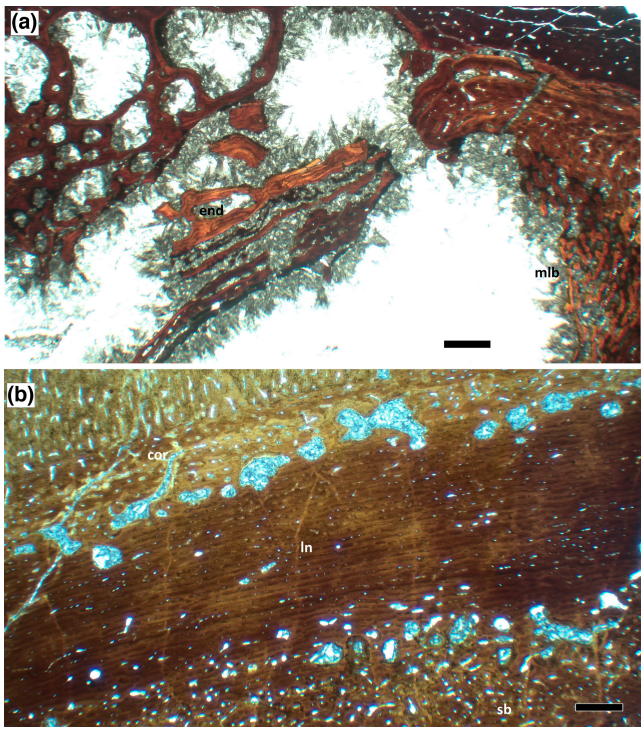

FIGURE 4 (a) Medullary cavity showing medullary bone-like deposition. (b) Detail of the "lens" of parallel fibered bone. cor, cortex; end, endosteal bone; ln, "lens" of parallel fibered bone; mlb, medullary bone-like tissue; sb, secondary bone. Scale bars = 500 μm.

overgrowth is also not compatible with an infectious etiology, particularly when considered in conjunction with the absence of draining sinuses (i.e. *cloacae*).

As such, fracture callus formation following a major traumatic lesion is the most probable remaining diagnosis to consider. The dome-like overgrowth is characterized by rapidly growing and highly vascularized primary bone, a tissue which can be found in fracture-related callus. The radial/perpendicular orientation of the pathological woven bone is similar to those previously reported in an injured fibula of *Psittacosaurus* (Hedrick et al., 2016) and fractured hadrosaurid ribs (Straight et al., 2009), suggesting a similar healing process in Cerapoda (the clade comprising these taxa). In humans, complete healing of an uncomplicated, non-displaced fracture in young individuals usually happens by the 16th week of healing (Rothschild & Martin, 2006), and well-formed callus, usually forms 3–4 weeks after such an injury occurs (Lovell, 1997; Marsell & Einhorn, 2011). These features all suggest that the overgrowth on the femur is a chronic fracture callus.

A limitation of this interpretation, however, is the lack of a clear fracture line in either the sections or the microtomographies, and this could contrast with the developmental stage of the overgrowth. It is possible that the fossilization processes introduced artifacts that make fracture identification difficult (cf. occasional detection of neurocentral or cranial sutures in other fossils). The time of repair/healing varies between modern animals, with a longer period occurring in reptiles compared to that required in birds and mammals (Hedrick et al., 2016, and references therein). In the absence of a specific medical history, however, only an approximate estimation of the duration of a fracture callus can be estimated. The development of the periosteal overgrowth suggests the animal survived for some time, but the exact time of death following the injury is impossible to determine.

4.2 | The presence of endosteal bone growth reaction in the pathological area

A cancellous and heterogeneous type of woven and endosteal tissue is located in the medullary cavity of the femur in the area covered by the overgrowth (Figures 3a and 4a). This diminishes away (proximally and distally) from the pathological region, corresponding to the apparently healthy regions of the bone, not affected by the overgrowth (section "A"). In the CT scans, the typical endosteal bone is recognized in the medial side of the medullary cavity, whereas the abnormal endosteal structure is distributed in the area immediately adjacent to the overgrowth, on the lateral side of the cavity (Figure 6b). The tissue is composed of primary woven bone that is highly vascularized and apparently similar to avian medullary bone. The latter is a bone tissue mainly deposited in the long bones of birds during the preovulatory cycle and is estrogen-dependent (Canoville et al., 2019; Schlumberger, 1959). It acts as a supply of calcium used to build the eggshell (Prondvai, 2016) and its presence is thus highly suggestive of a sexually mature female individual. The tissue has been used as a proxy to identify sexes in avian and non-avian dinosaurs (Hübner, 2012; Lee & Werning, 2008; Schweitzer et al., 2005, 2016) but was later proposed to also be correlated to other biological conditions such as certain diseases or injuries, e.g. osteopetrosis (Cerda et al., 2014; Chinsamy & Tumarkin-Deratzian, 2009; Prondvai, 2016), or even for a non-reproductive and non-pathological function (Prondvai & Stein, 2014). In fact, an endosteal tissue with a microstructure similar to the medullary bone can also be detected in pathological bones of birds (Canoville et al., 2020), and the distinction between the two tissues in the fossil record, especially for isolated/fragmentary materials, is still complicated (Canoville et al., 2021). The distribution and characteristics of the endosteal, medullary bone-like tissue along the shaft of the iguanodontian femur resembles that seen in the pathological humerus of *Larus argentatus* NCSM-19601 (Canoville et al., 2020) and in the femur of *Mussaurus patagonicus* (Cerda et al., 2014), suggesting that a pathological endosteal bone was deposited in the medullary region of the bone. This finding further emphasizes the importance of adopting a cautious approach when hypothesizing about the presence of ovulatory medullary bone, especially in isolated or fragmentary dinosaur bones.

4.3 | Muscular reconstruction and locomotory implications

The overgrowth, likely corresponding to a trauma on the thigh of the iguanodontian, is located on the distal craniolateral region of

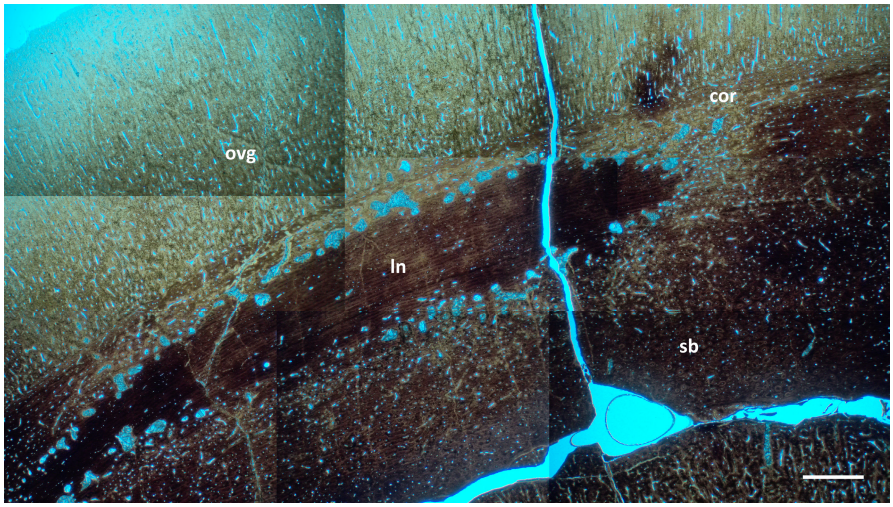

FIGURE 5 Composite picture showing the full extent of the "lens" of parallel fibered bone, located just below the cortex and the pathological periosteal overgrowth. cor, cortex; ln, "lens" of parallel fibered bone; ovg, overgrowth; sb, secondary bone. Scale bars = 2000 μm.

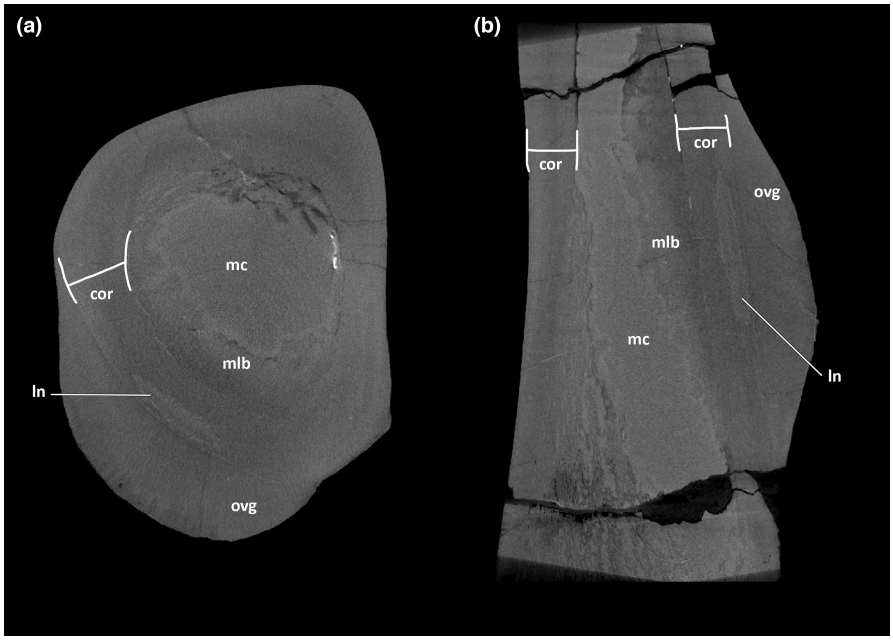

FIGURE 6 CT scans of the pathological area of NHMUK PV R6609, respectively in cross (a) and longitudinal (b) sections. The medullary cavity is hollow and irregularly sparse medullary bone-like tissue is present inside. The "lens" of parallel fibered bone placed below the periosteal overgrowth might represent a fragment of cortical bone following a blunt trauma. cor, cortex; ln, "lens" of compact bone; mc, medullary cavity; mlb, medullary bone-like tissue; ovg, overgrowth.

the femur, below the line of the fourth trochanter and above the point of caudal angulation of the distal section of the bone. Based on previous muscular reconstructions (Dilkes, 2000; Maidment & Barrett, 2012; Norman, 1986; Romer, 1927), the focal pathology would have been covered by the distal fascia, perhaps the tendinous cup, of the *M. triceps femoris* (formed by the inner *M. ambiens* and *M. femorotibialis*, and the superficial *M. iliotibialis*) and *M. iliofibularis* (Figure 2g).

M. triceps femoris originates along the dorsally raised margin of the ilium, inserting onto the cnemial crest of the tibia via a patellar tendon commune to its three sections (Norman, 1986), passing above the pathological overgrowth. *M. iliotibialis*, which forms the main part of the triceps femoris, is separated into *M. iliotibialis 1* (located cranially) and *M. iliotibialis 2* (located caudally, and greater in size than M. *iliotibialis 1*). *M. ambiens* is a small muscular fascia that originates on the proximal portion of the pubis, in front

of the acetabulum but before the pubic neck begins to develop (Norman, 1986; Romer, 1927). *M. femorotibialis* occupies the distal region of the femur in its medial (*M. femorotibialis medialis*) and lateral (*M. femorotibialis lateralis*) surfaces (Bates et al., 2012; Maidment & Barrett, 2012). *M. iliofibularis* is located ventrally to and separated from the *M. triceps femoris* and is assumed to originate on the lateral surface of the post-acetabular process of the ilium, inserting onto the proximolateral surface of the fibula (Dilkes, 2000).

M. iliotibialis 1, *M. iliotibialis 2*, *M. ambiens* and *M. femorotibialis* work in concert as *M. triceps femoris* extends the knee, while it is flexed by *M. iliofibularis* (Carrano & Hutchinson, 2002). The *M. iliotibialis 1* and *M. ambiens* could have aided the flexion of the femur (protraction) together with the *M. puboischiofemoralis externus* (Bates et al., 2012). *M. iliofibularis* and the caudal portion of the *M. triceps femoris*, together with other muscles (*M. caudofemoralis brevis*, *M. caudofemoralis longus* and *flexor cruris*) could have retracted the femur, extending the hip (Bates et al., 2012). In summary, the location of the pathological overgrowth is at a key position for movement of the lower thigh, particularly extension and flexion of the tibia, and protraction of the distal femur since it corresponds to the communal patellar tendon. The etiology of the injury cannot be precisely identified as it likely corresponds to a single traumatic impact, such as a fall to the ground, a blow from another individual (e.g. another iguanodontian or a predator) or some other environmental factors (e.g. Bertozzo et al., 2021). It is clear that the trauma could have negatively affected the musculature and locomotory capabilities of the individual. Similar direct blunt force trauma injuries in the proximity of the knee in humans, which also result in muscle contusions, can cause stiffness and restriction of movement of the knee (Bencardino et al., 2000; Dhillon et al., 2005). The area above the patella, overlain by the thin distal sheaths of *M. triceps femoralis*, appears to be thinner compared to the central and proximal regions of the femur, which is covered by the thick upper musculature. Major limb trauma at this point results in weakness of the quadriceps (formed by the homologous muscles of *M. triceps femoralis* and *M. iliofibularis*) in humans (Hennrikus et al., 1993), and it can be hypothesized that NHMUK PV R6609 had a limp, possibly putting it at increased risk of predation. Further ecological reconstructions cannot be offered at this time, however, due to the absence of additional skeletal material from the individual.

5 | CONCLUSIONS

Paleopathological lesions can reveal much about the diseases and injuries of fossilized individuals, offering a glimpse into their lifestyle and general response to traumatic events or diseases. NHMUK PV R6609 is a femur from an early adult Iguanodontia indet. individual, presenting a large and well-developed periosteal overgrowth, here diagnosed as evidence of a traumatic callus secondary to a knee injury. Analysis of CT scans and histological sections show no evidence of an *intra vitam* fracture line, but a "lens" of parallel-fibered bone is located near the external cortex, adjacent to the area of the periosteal overgrowth. This may be a bone fragment that was previously broken and later became encased within the healing region and is also suggestive of a blunt force trauma. The site of the injury corresponds to the initial development of the commune patellar tendon, which comprises the distal fascia of *M. triceps femoralis* (formed by *M. iliotibialis 1*, *M. iliotibialis 2*, *M. ambiens* and *M. femorotibialis*) and *M. iliofibularis*, and it might have negatively influenced the animal's locomotion, causing stiffness and weakness to the knee joint. The injury may have caused the dinosaur to limp and perhaps contributed to its death since it would have made it easier prey for predators.

The histological analysis confirmed the traumatic origin of the overgrowth of the femur, with an internal organization of pathological tissue similar to those already reported in injuries in *Psittacosaurus* and hadrosaurids (Hedrick et al., 2016; Straight et al., 2009). A peculiar structure comprising endosteal, trabecular and woven bone tissue evident in the medullary cavity is reminiscent of avian medullary bone, usually associated with females in pre-ovulatory stages. However, recent works (e.g. Canoville et al., 2020) have noted similarities between avian medullary bone and the endosteal tissue visible in pathological bones in birds and the difficulties of reliably differentiating between the two forms in the absence of histochemical analyses and the presence of medullary bone in paired bones (e.g. left and right femora). In fact, it has been suggested that ovulatory medullary bone can only be recognized by the presence of keratan sulfate and its deposition in paired elements (Canoville et al., 2021), proxies that cannot be applied to NHMUK PV R6609. Previous reports of abnormal endosteal bone have associated such tissue with pathological conditions, as in *Mussaurus* (Cerda et al., 2014). The similarities evident between the tissue in *Mussaurus* and NHMUK PV R6609 suggest it is highly likely that the bone tissue in the medullary cavity is directly related to the pathological condition of the bone. Future histological analyses of traumatic bones in other ornithischian clades (e.g. Stegosauria, Ankylosauridae, Pachycephalosauridae), similar to those undertaken in this study, may help determine if they share a similar healing process to Cerapoda (with large, fast-growing calluses). Such comparative analysis might reveal the occurrence of distinctive strategies between taxa living in different habitats and being selected under different ecological pressures. For example, the complex armed coverage of Ankylosauria might have served as a different calcium supply, aiding callus formation and resorption and leading to a different mode and tempo of healing than in ornithopod dinosaurs.

AUTHOR CONTRIBUTIONS

Conceptualization: FB. *Data curation*: FB, KS, and EV. *Formal analysis*: FB, KS, EV, FMG, and EM. *Investigation*: FB, KS, EV, FMG, AR, and EM. *Methodology*: FB and KS. *Resources*: FB. *Supervision*: AR and EM. *Visualization*: FB, KS, EV, FMG, AR, and EM. *Writing—original draft*: FB. *Writing—review & editing*: FB, KS, EV, FMG, AR, and EM.

ACKNOWLEDGEMENTS

We wish to thank Dr Susannah Maidment (NHMUK) for her professional and kind help during the collection survey at NHMUK, as well

as the assistance provided for the analytical aspects of this project (histological sectioning and CT scanning). Histological sections were made by Callum Hatch and Amy Scott-Murray (NHMUK). Our thanks go to Dr João Vasco Leite, Dr Paul Barrett, Joe Bonsor (NHMUK) and Dr Pascal Godefroit (Royal Belgian Institute of Natural Sciences, Belgium) for all the logistical help and discussions. Dr Maidment and Dr Gareth Arnott (QUB) provided insightful comments and suggestions to improve the manuscript. We are thankful to three anonymous reviewers for the comments and edits that greatly improved the manuscript. This research was undertaken as part of FB's doctoral dissertation within the Horizon 2020 research and innovation programme under the MSCA grant agreement no. 754507 (QUB SPaRK Cohort). All authors confirm there are no conflicts of interest to disclose.

DATA AVAILABILITY STATEMENT

The specimen, CT scans, and thin sections of the femur NHMUK PV R6609 are all curated in the collections of the Natural History Museum, London.

ORCID

Filippo Bertozzo https://orcid.org/0000-0002-0917-9989
Koen Stein https://orcid.org/0000-0003-4246-3225
Elena Varotto https://orcid.org/0000-0001-6637-9402
Francesco M. Galassi https://orcid.org/0000-0001-8902-3142
Alastair Ruffell https://orcid.org/0000-0001-6072-501X
Eileen Murphy https://orcid.org/0000-0003-0109-5817

REFERENCES

Anné, J., Hedrick, B.P. & Schein, J.P. (2016) First diagnosis of septic arthritis in a dinosaur. *Royal Society Open Science*, 3, 160222.

Bates, K.T., Maidment, S.C., Allen, V. & Barrett, P.M. (2012) Computational modelling of locomotor muscle moment arms in the basal dinosaur *Lesothosaurus diagnosticus*: assessing convergence between birds and basal ornithischians. *Journal of Anatomy*, 220, 212–232.

Bencardino, J.T., Rosenberg, Z.S., Brown, R.R., Hassankhani, A., Lustrin, E.S. & Beltran, J. (2000) Traumatic musculotendinous injuries of the knee: diagnosis with MR imaging. *Radiographics*, 20, 103–120.

Bertozzo, F., Bolotsky, I., Bolotsky, Y.L., Poberezhskiy, A., Ruffell, A., Godefroit, P. et al. (2022) A pathological ulna of *Amurosaurus riabinini* from the upper cretaceous of far eastern Russia. *Historical Biology*, 35, 268–275.

Bertozzo, F., Dal Sasso, C., Fabbri, M., Manucci, F. & Maganuco, S. (2017) Redescription of a remarkably large *Gryposaurus notabilis* (Dinosauria: Hadrosauridae) from Alberta, Canada. *Società Italiana di Scienze Naturali e Museo Civico di Storia Naturale*, XLIII, 1–56.

Bertozzo, F., Dalla Vecchia, F.M. & Fabbri, M. (2017) The Venice specimen of *Ouranosaurus nigeriensis* (Dinosauria, Ornithopoda). *PeerJ*, 5, e3403.

Bertozzo, F., Manucci, F., Dempsey, M., Tanke, D.H., Evans, D.C., Ruffell, A. et al. (2021) Description and etiology of paleopathological lesions in the type specimen of *Parasaurolophus walkeri* (Dinosauria: Hadrosauridae), with proposed reconstructions of the nuchal ligament. *Journal of Anatomy*, 238, 1055–1069.

Brown, C.M., Currie, P.J. & Therrien, F. (2021) Intraspecific facial bite marks in tyrannosaurids provide insight into sexual maturity and evolution of bird-like intersexual display. *Paleobiology*, 48, 12–43.

Butler, R.J., Yates, A.M., Rauhut, O.W. & Foth, C. (2013) A pathological tail in a basal sauropodomorph dinosaur from South Africa: evidence of traumatic amputation? *Journal of Vertebrate Paleontology*, 33, 224–228.

Canoville, A., Schweitzer, M.H. & Zanno, L.E. (2019) Systemic distribution of medullary bone in the avian skeleton: ground truthing criteria for the identification of reproductive tissues in extinct Avemetatarsalia. *BMC Evolutionary Biology*, 19, 1–20.

Canoville, A., Schweitzer, M.H. & Zanno, L.E. (2020) Identifying medullary bone in extinct avemetatarsalians: challenges, implications and perspectives. *Philosophical Transactions of the Royal Society B*, 375, 20190133.

Canoville, A., Zanno, L.E., Zheng, W. & Schweitzer, M.H. (2021) Keratan sulfate as a marker for medullary bone in fossil vertebrates. *Journal of Anatomy*, 238, 1296–1311.

Carrano, M.T. & Hutchinson, J.R. (2002) Pelvic and hindlimb musculature of *Tyrannosaurus rex* (Dinosauria: Theropoda). *Journal of Morphology*, 253, 207–228.

Cerda, I.A., Pol, D. & Chinsamy, A. (2014) Osteohistological insight into the early stages of growth in *Mussaurus patagonicus* (Dinosauria, Sauropodomorpha). *Historical Biology*, 26, 110–121.

Chinsamy, A. & Tumarkin-Deratzian, A. (2009) Pathologic bone tissues in a Turkey vulture and a nonavian dinosaur: implications for interpreting endosteal bone and radial fibrolamellar bone in fossil dinosaurs. *The Anatomical Record: Advances in Integrative Anatomy and Evolutionary Biology: Advances in Integrative Anatomy and Evolutionary Biology*, 292, 1478–1484.

Cruzado-Caballero, P., Díaz-Martínez, I., Rothschild, B., Bedell, M. & Pereda-Suberbiola, X. (2020) A limping dinosaur in the Late Jurassic: pathologies in the pes of the neornithischian *Othnielosaurus consors* from the Morrison Formation (Upper Jurassic, USA). *Historical Biology*, 33, 1753–1759.

Cruzado-Caballero, P., Lecuona, A., Cerda, I. & Diaz-Martinez, I. (2021) Osseous paleopathologies of Bonapartesaurus rionegrensis (Ornithopoda, Hadrosauridae) from Allen Formation (Upper Cretaceous) of Patagonia Argentina. *Cretaceous Research*, 124, 104800.

Dalla Vecchia, F.M. (2009) Tethyshadros insularis, a new hadrosauroid dinosaur (Ornithischia) from the Upper Cretaceous of Italy. *Journal of Vertebrate Paleontology*, 29, 1100–1116.

de Buffrénil, V. & Quilhac, A. (2021) Bone tissue types: a brief account of currently used categories. In: de Buffrénil, V., de Ricqlès, A.J., Zylberberg, L. & Padian, K. (Eds.) *Vertebrate skeletal histology and paleohistology*. Boca Raton, FL: CRC Press, pp. 147–190.

de Souza Barbosa, F.H., Da Costa, P.V.L.G., Bergqvist, L.P. & Rothschild, B.M. (2016) Multiple neoplasms in a single sauropod dinosaur from the Upper Cretaceous of Brazil. *Cretaceous Research*, 62, 13–17.

Dhillon, M.S., Panday, A.K., Aggarwal, S. & Nagi, O.N. (2005) Extra articular arthroscopic release in post-traumatic stiff knees: a prospective study of endoscopic quadriceps and patellar release. *Acta Orthopaedica Belgica*, 71, 197–203.

Dilkes, D.W. (2000) Appendicular myology of the hadrosaurian dinosaur *Maiasaura peeblesorum* from the Late Cretaceous (Campanian) of Montana. *Earth and Environmental Science Transactions of the Royal Society of Edinburgh*, 90, 87–125.

Dumbravă, M.D., Rothschild, B.M., Weishampel, D.B., Csiki-Sava, Z., Andrei, R.A., Acheson, K.A. et al. (2016) A dinosaurian facial deformity and the first occurrence of ameloblastoma in the fossil record. *Scientific Reports*, 6, 29271.

Ekhtiari, S., Chiba, K., Popovic, S., Crowther, R., Wohl, G., Kin On Wong, A. et al. (2020) First case of osteosarcoma in a dinosaur: a multimodal diagnosis. *The Lancet. Oncology*, 21, 1021–1022.

Farke, A.A. & O'Connor, P.M. (2007) Pathology in *Majungasaurus crenatissimus* (Theropoda: abelisauridae) from the Late Cretaceous of Madagascar. *Journal of Vertebrate Paleontology*, 27, 180–184.

Farke, A.A., Wolff, E.D.S. & Tanke, D.H. (2009) Evidence of combat in *Triceratops*. *PLoS One*, 4, e4252.

Foth, C., Evers, S.W., Pabst, B., Mateus, O., Flisch, A., Patthey, M. et al. (2015) New insights into the lifestyle of *Allosaurus* (Dinosauria:

Theropoda) based on another specimen with multiple pathologies. *PeerJ*, 3, e940.

García, R.A., Cerda, I.A., Heller, M., Rothschild, B.M. & Zurriaguz, V. (2017) The first evidence of osteomyelitis in a sauropod dinosaur. *Lethaia*, 50, 227–236.

Godefroit, P., Dong, Z.M., De Potter, H., Lenglet, G. & Smith, T. (1998) Sino-Belgian cooperation program cretaceous dinosaurs and mammals from inner Mongolia. 1. New *Bactrosaurus* (Dinosauria: Hadrosauroidea) material from Iren Dabasu (inner Mongolia, Pr China). *Bulletin de l'Institut Royal des Sciences Naturelles de Belgique: Sciences de la Terre*, 68, 3–70.

Gonzalez, R., Gallina, P.A. & Cerda, I.A. (2017) Multiple paleopathologies in the dinosaur *Bonitasaura salgadoi* (Sauropoda: Titanosauria) from the Upper Cretaceous of Patagonia, Argentina. *Cretaceous Research*, 79, 159–170.

Griffin, C.T. (2018) Pathological bone tissue in a Late Triassic neotheropod fibula, with implications for the interpretation of medullary bone. *New Jersey State Museum Investigations*, 6, 2–10.

Gutherz, S.B., Groenke, J.R., Sertich, J.J., Burch, S.H. & O'connor, P.M. (2020) Paleopathology in a nearly complete skeleton of *Majungasaurus crenatissimus* (Theropoda: Abelisauridae). *Cretaceous Research*, 115, 104553.

Hamm, C.A., Hampe, O., Schwarz, D., Witzmann, F., Makovicky, P.J., Brochu, C.A. et al. (2020) A comprehensive diagnostic approach combining phylogenetic disease bracketing and CT imaging reveals osteomyelitis in a *Tyrannosaurus rex*. *Scientific Reports*, 10, 1–16.

Hanna, R.R. (2002) Multiple injury and infection in a sub-adult theropod dinosaur *Allosaurus fragilis* with comparisons to allosaur pathology in the Cleveland-Lloyd Dinosaur Quarry Collection. *Journal of Vertebrate Paleontology*, 22, 76–90.

Hedrick, B.P., Gao, C., Tumarkin-Deratzian, A.R., Shen, C., Holloway, J.L., Zhang, F. et al. (2016) An injured *Psittacosaurus* (Dinosauria: Ceratopsia) from the Yixian Formation (Liaoning, China): implications for *Psittacosaurus* biology. *The Anatomical Record*, 299, 897–906.

Hennrikus, W.L., Kasser, J.R., Rand, F., Millis, M.B. & Richards, K.M. (1993) The function of the quadriceps muscle after a fracture of the femur in patients who are less than seventeen years old. *The Journal of Bone and Joint Surgery*, 75, 508–513.

Hübner, T.R. (2012) Bone histology in *Dysalotosaurus lettowvorbecki* (Ornithischia: Iguanodontia)—variation, growth, and implications. *PLoS One*, 7, e29958.

Hunt, T.C., Peterson, J.E., Frederickson, J.A., Cohen, J.E. & Berry, J.L. (2019) First documented pathologies in *Tenontosaurus tilletti* with comments on infection in non-avian dinosaurs. *Scientific Reports*, 9, 1–8.

Jentgen-Ceschino, B., Stein, K. & Fischer, V. (2020) Case study of radial fibrolamellar bone tissues in the outer cortex of basal sauropods. *Philosophical Transactions of the Royal Society B*, 375, 20190143.

Lee, A.H. & Werning, S. (2008) Sexual maturity in growing dinosaurs does not fit reptilian growth models. *Proceedings of the National Academy of Sciences of the United States of America*, 105, 582–587.

Lovell, N.C. (1997) Trauma analysis in paleopathology. *Yearbook of Physical Anthropology*, 40, 139–170.

Maidment, S.C. & Barrett, P.M. (2012) Does morphological convergence imply functional similarity? A test using the evolution of quadrupedalism in ornithischian dinosaurs. *Proceedings of the Royal Society B: Biological Sciences*, 279, 3765–3771.

Mansour, M., Adi, M., Mousa, H., Haroun, N., Rustum, M., Joha, M. et al. (2023) A post-traumatic ossified subdural chronic hematoma successfully managed in a 34-year-old woman: a case report. *Annals of Medicine and Surgery*, 85, 1026–1029.

Marsell, R. & Einhorn, T.A. (2011) The biology of fracture healing. *Injury*, 42, 551–555.

Martinelli, A.G., Teixeira, V.P., Marinho, T.S., Fonseca, P.H., Cavellani, C.L., Araujo, A.J. et al. (2015) Fused mid-caudal vertebrae in the titanosaur *Uberabatitan ribeiroi* from the Late Cretaceous of Brazil and other bone lesions. *Lethaia*, 48, 456–462.

McDonald, A.T. (2012) Phylogeny of basal iguanodonts (Dinosauria: Ornithischia): an update. *PLoS One*, 7, e36745.

McDonald, A.T., Bird, J., Kirkland, J.I. & Dodson, P. (2012) Osteology of the basal hadrosauroid *Eolambia caroljonesa* (Dinosauria: Ornithopoda) from the Cedar Mountain Formation of Utah. *PLoS One*, 7(10), e45712.

Mitchell, J., Sander, P.M. & Stein, K. (2017) Can secondary osteons be used as ontogenetic indicators in sauropods? Extending the histological ontogenetic stages into senescence. *Paleobiology*, 43, 321–342.

Moodie, R.L. (1923) *Paleopathology: an introduction to the study of ancient evidences of disease*. Champaign, IL: University of Illinois Press.

Norman, D.B. (1980) On the ornithischian dinosaur *Iguanodon bernissartensis* from the Lower Cretaceous of Bernissart (Belgium). *Memorie de l'Institut Royal Des Sciences Naturelles de Belgique*, 178, 1–105.

Norman, D.B. (1986) On the anatomy of *Iguanodon atherfieldensis* (Ornithischia: Ornithopoda). *Bulletin de l'Institut Royal des Sciences Naturelles de Belgique: Sciences de la Terre*, 56, 281–372.

Norman, D.B. (2002) On Asian ornithopods (Dinosauria: Ornithischia). 4. *Probactrosaurus*. *Zoological Journal of the Linnean Society*, 136, 113–144.

Peterson, J.E., Dischler, C. & Longrich, N.R. (2013) Distributions of cranial pathologies provide evidence for head-butting in dome-headed dinosaurs (Pachycephalosauridae). *PLoS One*, 8, e68620.

Peterson, J.E. & Vittore, C.P. (2012) Cranial pathologies in a specimen of *Pachycephalosaurus*. *PLoS One*, 7, e36227.

Prondvai, E. (2016) Medullary bone in fossils: function, evolution and significance in growth curve reconstructions of extinct vertebrates. *Journal of Evolutionary Biology*, 30, 440–460.

Prondvai, E. & Stein, K.H. (2014) Medullary bone-like tissue in the mandibular symphyses of a pterosaur suggests non-reproductive significance. *Scientific Reports*, 4, 6253.

Redelstorff, R., Hayashi, S., Rothschild, B.M. & Chinsamy, A. (2014) Non-traumatic bone infection in *Stegosaurs* from Como Bluff, Wyoming. *Lethaia*, 48, 47–55.

Romer, A.S. (1927) The pelvic musculature of ornithischian dinosaurs. *Acta Zoologica*, 8, 225–275.

Rothschild, B.M. & Berman, D.S. (1991) Fusion of caudal vertebrae in Late Jurassic sauropods. *Journal of Vertebrate Paleontology*, 11, 29–36.

Rothschild, B.M. & Martin, L.D. (2006) Skeletal impact of disease. *New Mexico Museum of Natural History and Science*, 33, 1–226.

Rothschild, B.M., Tanke, D., Rühli, F., Pokhojaev, A. & May, H. (2020) Suggested case of Langerhans cell histiocytosis in a cretaceous dinosaur. *Scientific Reports*, 10, 1–10.

Schlumberger, H.G. (1959) Polyostotic hyperostosis in the female parakeet. *The American Journal of Pathology*, 35, 1–23.

Schweitzer, M.H., Wittmeyer, J.L. & Horner, J.R. (2005) Gender-specific reproductive tissue in ratites and *Tyrannosaurus rex*. *Science*, 308, 1456–1460.

Schweitzer, M.H., Zheng, W., Zanno, L., Werning, S. & Sugiyama, T. (2016) Chemistry supports the identification of gender-specific reproductive tissue in *Tyrannosaurus rex*. *Scientific Reports*, 6, 1–10.

Senter, P. & Juengst, S.L. (2016) Record-breaking pain: the largest number and variety of forelimb bone maladies in a theropod dinosaur. *PLoS One*, 11, e0149140.

Siviero, B.C., Rega, E., Hayes, W.K., Cooper, A.M., Brand, L.R. & Chadwick, A.V. (2020) Skeletal trauma with implications for intratail mobility in *Edmontosaurus annectens* from a monodominant bonebed, Lance Formation (Maastrichtian), Wyoming USA. *PALAIOS*, 35, 201–214.

Słowiak, J., Szczygielski, T., Rothschild, B.M. & Surmik, D. (2021) Dinosaur senescence: a hadrosauroid with age-related diseases brings a new perspective of "old" dinosaurs. *Scientific Reports*, 11(1), 11947.

Straight, W.H., Davis, G.L., Skinner, H.C.W., Haims, A., Mcclennan, B.L. & Tanke, D.H. (2009) Bone lesions in hadrosaurs: computed

tomographic imaging as a guide for paleohistologic and stable-isotopic analysis. *Journal of Vertebrate Paleontology*, 29, 315–325.

Tanke DH, Rothschild BM. 2014. Paleopathology in late *Cretaceous hadrosauridae* from Alberta, Canada. In: Eberth DA, Evans DC, editors. *Hadrosaurs. Life of the past*. Bloomington: Indiana University Press; p. 540–571.

Tschopp, E., Wings, O., Frauenfelder, T. & Rothschild, B.M. (2014) Pathological phalanges in a camarasaurid sauropod dinosaur and implications on behaviour. *Acta Palaeontologica Polonica*, 61, 125–134.

Verdú, F.J., Godefroit, P., Royo-Torres, R., Cobos, A. & Alcalá, L. (2017) Individual variation in the postcranial skeleton of the early cretaceous *Iguanodon bernissartensis* (Dinosauria: Ornithopoda). *Cretaceous Research*, 74, 65–86.

Witzmann, F., Hampe, O., Rothschild, B.M., Joger, U., Kosma, R., Schwarz, D. et al. (2016) Subchondral cysts at synovial vertebral joints as analogies of Schmorl's nodes in a sauropod dinosaur from Niger. *Journal of Vertebrate Paleontology*, 36, e1080719.

Woodward, H.N., Freedman Fowler, A.E., Farlow, J.O. & Horner, J.R. (2015) *Maiasaura*, a model organism for extinct vertebrate population biology: a large sample statistical assessment of growth dynamics and survivorship. *Paleobiology*, 41, 503–527.

Wosik, M., Chiba, K., Therrien, F. & Evans, D.C. (2020) Testing size–frequency distributions as a method of ontogenetic aging: a life-history assessment of hadrosaurid dinosaurs from the Dinosaur Park Formation of Alberta, Canada, with implications for hadrosaurid paleoecology. *Paleobiology*, 46, 379–404.

Wosik, M. & Evans, D.C. (2022) Osteohistological and taphonomic life-history assessment of *Edmontosaurus annectens* (Ornithischia: Hadrosauridae) from the Late Cretaceous (Maastrichtian) Ruth Mason dinosaur quarry, South Dakota, United States, with implication for ontogenetic segregation between juvenile and adult hadrosaurids. *Journal of Anatomy*, 241, 272–296.

How to cite this article: Bertozzo, F., Stein, K., Varotto, E., Galassi, F.M., Ruffell, A. & Murphy, E. (2024) Histological analysis and etiology of a pathological iguanodontian femur from England. *Journal of Anatomy*, 00, 1–11. Available from: https://doi.org/10.1111/joa.14053